International Journal of Heat and Technology
Vol. 42, No. 3, June, 2024, pp. 721-730
Journal homepage: http://iieta.org/journals/ijht

Numerical Analysis of Heat Transfer Deterioration of Hydrogen Flowing in a Circular Pipe under Transcritical Boundary Conditions

Rafiq Manna[1*], Ahmad Al-Aboushi[1], Nabeel Abu Shaban[1], Ibraheem Nasser[2]

[1] Mechanical Engineering Department, Faculty of Engineering and Technology, Al-Zaytoonah University of Jordan, Amman 11733, Jordan
[2] Chair of Space Propulsion and Mobility, Technical University of Munich, Ottobrunn 85521, Germany

Corresponding Author Email: ibraheem.nasser@tum.de

https://doi.org/10.18280/ijht.420301

Received: 26 February 2024
Revised: 5 May 2024
Accepted: 17 May 2024
Available online: 27 June 2024

Keywords:
hydrogen, cooling channel, rocket engine, heat transfer deterioration, supercritical, gerg-2008 equation of state

ABSTRACT

In various systems, such as rocket engines, efficiency is improved by increasing the pressure so that these systems operate at extremely high supercritical pressures. At this pressure, pseudo-boiling occurs, and heat transfer deteriorates, suddenly decreasing when certain temperature limits are exceeded. This study numerically solved the Navier–Stokes equations for a circular cooling channel. In addition, supercritical hydrogen was used as a coolant. The thermophysical and transport properties were defined as a user-defined function in ANSYS FLUENT. The results showed that increasing the operating pressure significantly reduced the heat transfer deterioration, improved the cooling capabilities, and minimized pressure drops. Increasing the mass flow rate enhances the heat transfer but increases the pressure losses. The influence of the operating pressure and the mass flow rate on the deterioration of the heat transfer was investigated in detail.

1. INTRODUCTION

Regenerative cooling is a frequently utilized technique for cooling rocket engines. Nasser et al. [1-3] and can also be used with hydrogen as a coolant [4-8]. In regenerative cooling, the engine's hot combustion gases are passed through channels in of the combustion chamber wall. These channels are usually made of a material with good thermal conductivity, such as copper [9-13]. Hydrogen in-space propulsion systems and rocket engines offer several advantages and disadvantages. One advantage is its high specific impulse, i.e., it can deliver more thrust per unit of propellant compared to other options. In addition, hydrogen is readily available and can be quickly produced by water electrolysis. However, there are also disadvantages. Hydrogen is highly volatile and requires careful handling and storage due to its low density and tendency to leak [14].

In addition, the storage tanks need to be insulated to maintain the low temperature, which makes the system heavier and more complex. In addition, hydrogen combustion can produce water vapor, which can freeze at extremely low temperatures in space and damage the rocket. While hydrogen offers significant potential for space propulsion, the practical challenges associated with its handling and storage must be carefully considered. Xie and Zhang [15] have investigated a design with a spherical convex structure on the inner wall to improve cooling performance, reduce thermal stratification and protect against overheating. By optimizing the distance between the convexities, a balance between improved cooling performance and minimal pressure drop is achieved. Introducing the spherical convex surface increases the disturbance of the coolant flow, resulting in improved convective heat transfer efficiency. The findings indicate that utilizing a 0.2 mm deep spherical convex shape with a 2.5 mm pitch can enhance heat transfer efficiency and reduce thermal stratification within a channel measuring 2 mm ×2 mm in cross-section.

Gibreel et al. [16] and Elmouazen et al. [17] studied hydrogen's heat transfer and flow characteristics within a unique ribbed structure located in a branched, undulating cooling channel of a rocket motor combustion chamber. Their research involved numerical simulations utilizing varying gap widths and amplitudes. The findings demonstrated that the initial symmetric layout exhibited superior wall temperatures for heat transfer and average Nusselt numbers compared to the parallel layout. Additionally, the revised symmetric wavy design illustrated a substantial enhancement in Nusselt numbers within the secondary branch flow, attributed to enhanced fluid mixing among neighboring channels. A novel cooling configuration was developed by Xie and Zhang [18] that combines fins and spherical convex shapes. The results show that this new structure significantly reduces the maximum wall temperature and alleviates the problem of uneven fluid distribution. Compared to a smooth channel and a structure with only spherical convex shapes, the maximum temperature decreased by 18.4% and 10.3%, respectively, while the temperature non-uniformity index decreased by 25.1% and 20.8%, respectively.

In rocket engines with supercritical fluids, degradation of heat transfer can occur under certain conditions [19-21]. This phenomenon is primarily caused by the high heat flux in liquid rocket motors, leading to an increased heat-to-mass flow ratio.

However, it has been observed that the deterioration can be reduced if the pressure is well above the critical point and the engine walls have rough surfaces [22-25].

Haemisch et al. [6] and Haemisch et al. [20] conducted studies using both experiments and numerical simulations to examine heat transfer processes in the cooling channels utilizing LNG at supercritical conditions. The experiment was accomplished in a scaled-down combustion chamber separated into four branches around the rim, each equipped with rectangular cooling channels with various aspect ratios. Cooling fluids such as cryogenic hydrogen and liquid methane were utilized. These studies provided a comprehensive data set to validate computational fluid dynamics simulations to predict wall temperatures under high-pressure conditions. Thermal stratification impacts, which typically impair cooling efficiency in cooling channels with high aspect ratios, were observed for coolants. Nevertheless, these effects were much more pronounced for hydrogen than for methane. The simulations deviated significantly from the experimental results near the critical point where heat transfer decreases.

Tong et al. [26], Mardani and Barani [27] used numerical simulations to investigate the flow of supercritical hydrogen in a cylindrical and triangular U-tube neutron moderator. They investigated how different inlet tube heights affect the flow and heat transfer. The main outcome shows that while the dimensions of the vortex and the velocity gradient change with the ratio of height to diameter (H/D), the central position of the vortex remains stable regardless of the height variation. This indicates that the overall flow field tends to be consistent and stable. The most significant variation of the Reynolds number (was observed for the Nusselt number. The effects of the secondary flow on Nusselt number corresponded to the input effect of a straight pipe upstream, whereby the influence of the secondary flow on Nusselt number exceeded the input effect.

Tong et al. [26] investigated a GH2/LOX coaxial jet flame under transcritical and supercritical conditions using the RANS approach. The study shows that the flow pattern is influenced by two vortices created by the substantial expansion of the oxygen-dense core and the high velocity of the gaseous hydrogen entering the chamber. By increasing the chamber pressure, the transcritical conditions are retarded, leading to an increase in the flame length and the length of the secondary vortex and a reduction in the expansion zone. Furthermore, the two detailed chemical mechanisms proposed by Burke and Konnov lead to similar results. Zhang et al. [28]. Performed a numerical analysis to study the thermal behavior of cryogenic liquid hydrogen in storage tank during the transition from gas-liquid separation to a supercritical state. The simulation used a two-stage approach with different models. The results showed a significant increase in absolute pressure due to the non-uniform temperature distribution in the gas-liquid layer phase.

Consequently, increased heat flow exacerbated the non-uniform temperature distribution and shortened the safe storage time. The study also investigated the effects of heat flow and thermodynamic conditions on safe storage time. In addition, the critical state boundary's influence on the two-stage simulation's accuracy was investigated. It was found that the boundary condition defining the occurrence of a local supercritical state was superior to the other conditions considered in this study.

Hou et al. [29] utilized a molecular dynamics methodology to comparatively assess the characteristics of a liquid hydrogen propellant jet injection in spacecraft propulsion systems operating under subcritical and supercritical conditions. Their investigation revealed that under supercritical conditions, the rate of radial density change of the jet remains minimal. As a result, the surface area and volume of the liquid phase area of the jet were quantified and computed. When contrasted with the subcritical state, the volume of the liquid hydrogen jet decreased by 1.9% in the supercritical environment, while the surface area increased by 6.7%. Molecular stress analyses were conducted to elucidate the alterations in surface area caused by molecular diffusion. The study indicated that the stresses in the hydrogen jet under supercritical conditions were only 88.9% of those observed under subcritical conditions.

In this research, the impact of operating pressure, inlet temperature, and mass flow rate on heat transfer deterioration in transcritical hydrogen flow inside a tube is examined. The study employs numerical solutions of the Navier-Stokes equations carried out using ANSYS FLUENT [30]. In addition, hydrogen's thermophysical and transport properties are calculated using a GERG-2008 equation of state [31] and an extended model of the corresponding states [32], respectively. The article is organized as follows: Section 1 thoroughly reviews the existing literature. Section 2 deals with the physical model, including the equation of state and the conjugate heat transfer equation. This section also validates the numerical model and shows the results of lattice convergence. Section 3 concludes the paper with a presentation and discussion of the results.

2. EQUATION OF STATE

The GERG-2008 model [31] is the most accurate for hydrocarbons [33, 34]. It is suitable for both subcritical and supercritical conditions. Since the boundary conditions of the cooling channel in the present work maintain pressures below 32.5 bar and temperatures of 760 K for hydrogen, the GERG-2008 model is suitable. It is based on the interaction of Helmholtz free energy, temperature, pressure, and mole fraction. This free energy is split into two components, with one characterizing the ideal gas mixture properties and the other encapsulating the residual fraction properties.

$$\alpha(\delta, \tau, \bar{x}) = \alpha^{o}(\rho, T, \bar{x}) + \alpha^{r}(\delta, \tau, \bar{x}) \tag{1}$$

$$\alpha^{o}(\rho, T, \bar{x}) = \sum_{i=1}^{N} x_i \left[\alpha_{oi}^{o}(\rho, T) + \ln x_i\right] \tag{2}$$

$$\alpha^{r}(\delta, \tau, \bar{x}) = \sum_{i=1}^{N} x_i \alpha_{oi}^{r}(\delta, T) + \sum_{i=1}^{N-1} \sum_{j=i+1}^{N} x_i x_j F_{ij} \alpha_{ij}^{r}(\delta, \tau) \tag{3}$$

The remaining portion is divided into two more sections. The first section represents the remaining amount for each individual species, while the second section calculates the binary departure function for the mixture. The reduced density of the mixture and the inverse reduced temperature of the mixture are then determined as follows:

$$\delta = \frac{\rho}{\rho_r(H_2)} \tag{4}$$

$$\tau = \frac{T_r(H_2)}{T} \tag{5}$$

Kunz and Wagner [31] provides the binary parameters for species, coefficients, and derivatives of the reduced Helmholtz free energy relevant to the ideal-gas mixture and residual components associated with reduced temperature and density within the GERG-2008 model. Utilizing the various derivatives of the reduced Helmholtz free energy components allows for the computation of thermophysical properties for either a pure substance or a mixture. The determination of pressure and isobaric heat capacity can be carried out using the following calculations.

$$\frac{P(\delta, \tau, \bar{x})}{\rho R T} = 1 + \delta\alpha_{\delta}^{r} \tag{6}$$

$$\frac{c_p(\delta, \tau, \bar{x})}{R} = -\tau^2(\alpha_{\tau\tau}^{o} + \alpha_{\tau\tau}^{r}) + \frac{(1 + \delta\alpha_{\delta}^{r} - \delta\tau\alpha_{\delta\tau}^{r})^2}{1 + 2\delta\alpha_{\delta}^{r} + \delta^2\alpha_{\delta\delta}^{r}} \tag{7}$$

The ECS hypothesis, frequently referred to in the literature [32, 35-39], is often used to calculate fluid mixtures' viscosity and thermal conductivity. These properties are determined by considering the contributions of dilute gas, residues, and critical components. Each of these components interacts with the mixture based on its mole fraction.

$$\mu = \mu^{o}(T, \bar{x}) + \mu^{r}(T, \rho, \bar{x}) + \mu^{c}(T, \rho, \bar{x}) \tag{8}$$

$$k = k^{o}(T, \bar{x}) + k^{r}(T, \rho, \bar{x}) + k^{c}(T, \rho, \bar{x}) \tag{9}$$

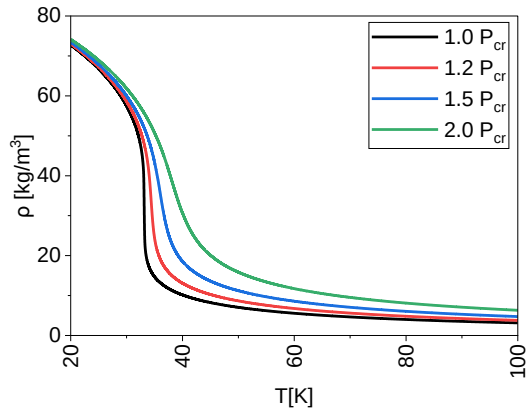

(a) Density

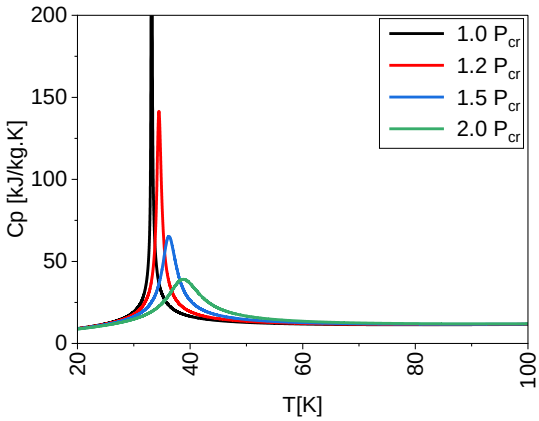

(b) Isobaric heat capacity

Figure 1. Thermophysical properties of hydrogen

Near the critical point, the density of hydrogen can be significantly affected by changes in pressure and temperature, as shown in Figure 1. As pressure increases, the density of hydrogen usually increases as well since the higher pressure compresses the hydrogen molecules, resulting in a higher packing density. As far as temperature is concerned, the density of hydrogen tends to decrease near the critical point as the temperature increases. As the temperature increases, the hydrogen molecules gain more kinetic energy, so they move further apart and occupy a larger volume, resulting in a lower density. Isobaric heat capacity refers to the amount of heat required to raise the temperature of a substance at constant pressure. Near the critical point and the pseudo boiling point, the isobaric heat capacity of hydrogen can be affected by changes in pressure and temperature, as shown in Figure 1. Under near-critical conditions, the intermolecular forces in the liquid become weaker, resulting in lower flow resistance and viscosity. As a result, supercritical hydrogen tends to have similar flow properties to gasses (see Figure 2). This low viscosity makes supercritical hydrogen suitable for various industrial applications, including power generation and extraction processes. The thermal conductivity of supercritical hydrogen near its critical point increases compared to its gaseous phase, as shown in Figure 2. This behavior is due to the increased density of the supercritical state and intermolecular interactions. As the temperature and pressure approach the critical point, the density of the liquid increases, resulting in more efficient heat transfer between the particles. Consequently, supercritical hydrogen has a higher thermal conductivity than its gaseous state.

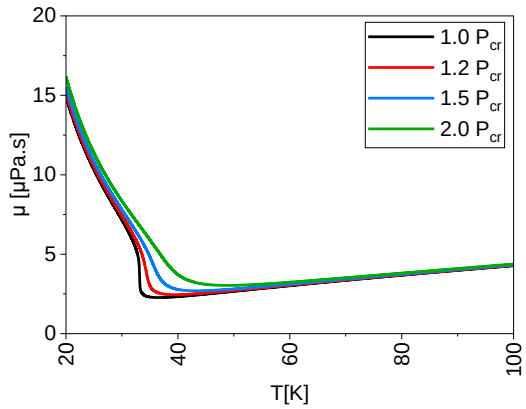

(a) Viscosity

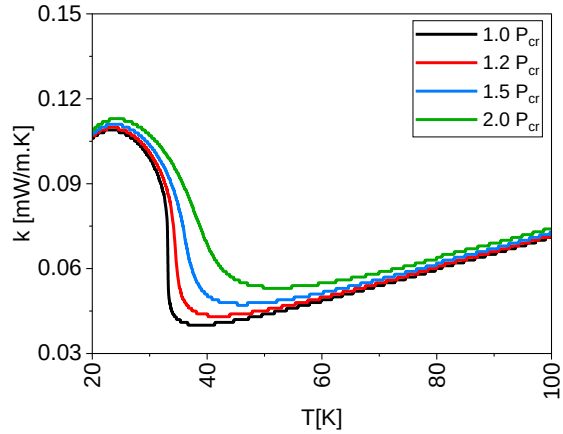

(b) Thermal conductivity

Figure 2. Transport properties of hydrogen

3. GOVERNING EQUATION

The governing equation represents a steady, compressible flow. CFD adopts the subsequent method to resolve the

conservation equations for mass, momentum, and energy using cylindrical notation.

Mass conservation:

$$\frac{\partial}{\partial x}(\rho u_x) + \frac{1}{r}\frac{\partial}{\partial r}(\rho r u_r) = 0 \tag{10}$$

Momentum conservation:

$$\frac{\partial}{\partial x}(\rho u_x u_x) + \frac{1}{r}\frac{\partial}{\partial r}(r\rho u_x u_r) = -\frac{\partial p}{\partial x} + \frac{\partial \tau_{xx}}{\partial x} + \frac{1}{r}\frac{\partial}{\partial r}(r\tau_{xr}) \tag{11}$$

$$\frac{\partial}{\partial x}(\rho u_r u_x) + \frac{1}{r}\frac{\partial}{\partial r}(r\rho u_r u_r) = -\frac{\partial p}{\partial r} + \frac{\partial \tau_{rx}}{\partial x} + \frac{1}{r}\frac{\partial}{\partial r}(r\tau_{rr}) \tag{12}$$

Energy conservation:

$$\rho C_p u_x \frac{\partial T}{\partial x} + \rho C_p u_r \frac{\partial T}{\partial r} = \frac{\partial}{\partial x}\left(\lambda_t \frac{\partial T}{\partial x}\right) + \frac{1}{r}\frac{\partial}{\partial r}\left(r\lambda_t \frac{\partial T}{\partial x}\right) - \frac{T}{\rho}\left(\frac{\partial \rho}{\partial T}\right)\vec{u} \cdot \nabla p \tag{13}$$

The viscous terms are defined as:

$$\tau_{rr} = \mu_{eff}\left[2\frac{\partial u_r}{r} - \frac{2}{3}(\nabla u)\right] \tag{14}$$

$$\tau_{xr} = \tau_{rx} = \mu_{eff}\left[\frac{\partial u_x}{\partial r} + \frac{\partial u_r}{\partial x}\right] \tag{15}$$

$$\nabla(u) = \frac{\partial u_x}{\partial x} + \frac{1}{r}\frac{\partial}{\partial r}(r u_r) \tag{16}$$

Employing an enhanced wall treatment in the near-wall region, the k-ε turbulence model proves effective in predicting the heat transfer characteristics of hydrogen under supercritical pressure conditions. The k-ε turbulence model equation [40] was implemented to address turbulent fluid flow accordingly.

$$\frac{\partial}{\partial x}(\rho u_x K) + \frac{1}{r}\frac{\partial}{\partial r}(r\rho u_x K) = \frac{\partial}{\partial x}\left[\left(\mu + \frac{\mu_t}{\sigma_k}\right)\frac{\partial K}{\partial x}\right] + \frac{1}{r}\frac{\partial}{\partial r}\left[\left(\mu + \frac{\mu_t}{\sigma_k}\right)\frac{\partial K}{\partial r}\right] - \rho\varepsilon + G_k + G_b \tag{17}$$

$$\frac{\partial}{\partial x}(\rho u_x \varepsilon) + \frac{1}{r}\frac{\partial}{\partial r}(r\rho u_x \varepsilon) = \frac{\partial}{\partial x}\left[\left(\mu + \frac{\mu_t}{\sigma_\varepsilon}\right)\frac{\partial \varepsilon}{\partial x}\right] + \frac{1}{r}\frac{\partial}{\partial r}\left[\left(\mu + \frac{\mu_t}{\sigma_k}\right)\frac{\partial \varepsilon}{\partial r}\right] + C_1\frac{\varepsilon}{k}(G_k + C_3 G_b) - C_2\rho\frac{\varepsilon^2}{k} \tag{18}$$

The CFD simulations in this study were carried out using the commercial software ANSYS FLUENT 21.0 [30]. The computational domain was divided into sections using a structured grid created with the commercial software ICEM CFD. A grid independence test was performed using the k-e model with improved wall treatment in a smooth pipe to ensure accuracy.

4. VALIDATION

In this validation study, experimental data sourced from NASA [41] were utilized to confirm the model's capability to accurately predict the reduction in heat transfer caused by elevated heat flux at supercritical pressures. The test setup was equipped with instruments to measure local temperature, pressure, and voltage, situated within a vacuum environment to minimize external heat transfer effects and electrically isolated from surrounding components. While most test sections displayed consistent heat flow without significant local resistance variations, one section featured a tapered wall to induce axial heat flux gradients akin to those in rocket engine cooling channels.

Pizzarelli [24] conducted a comparative analysis utilizing the same experimental data, investigating hydrogen flow in a heated tube at subcritical and supercritical pressures and temperatures. Multiple experiments were conducted, with test case "0294" selected for model validation. This specific test involved a pipe with an 8.5 mm inner diameter and a length of 91.44 cm, with heat flux applied at the pipe's end. The heat flow distribution is illustrated in Figure 3, with static pressure at the outlet recorded as 4.92 MPa, inlet temperature at 42.4 K, and a mass flow rate of 734 kg/m²s. The hydrogen flow in the pipe exhibited uniformity and axial symmetry.

For the simulation, a mesh size of 60×3000 (radial x upstream) was employed, utilizing radial clustering to maintain a y+ value under 1.0. A comparison between the numerical simulation, employing the k-ε turbulence model with enhanced wall treatment and representation of wall temperature, and the experimental data for test case 0294 is depicted in Figure 4. The results indicate agreement between the numerical simulation and experimental findings, showcasing the reliability of the k-ε turbulence model with enhanced wall treatment in elucidating heat transfer deterioration near the critical fluid flow region.

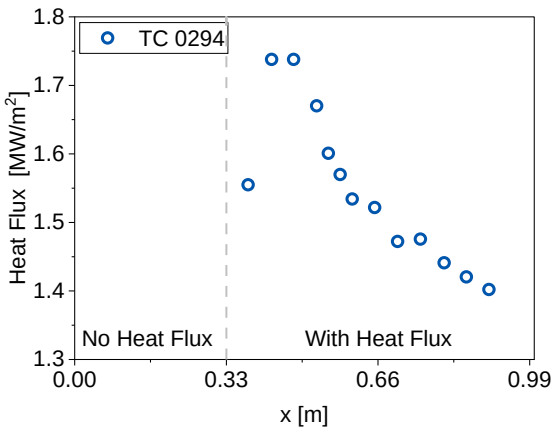

Figure 3. Heat flux distribution

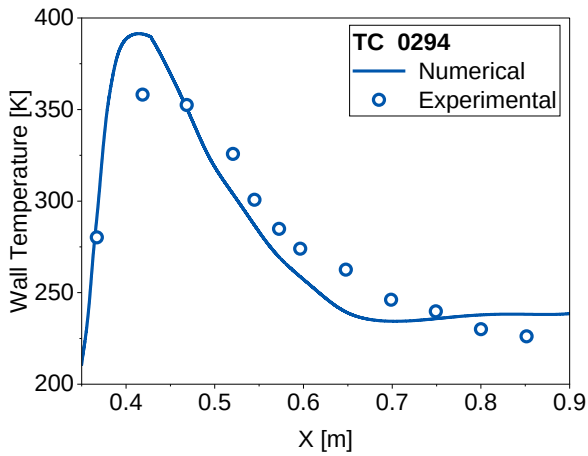

Figure 4. Wall temperature validation

5. NUMERICAL ANALYSIS

5.1 Physical model

In this study, different operating pressures and mass flows for hydrogen near the critical point are investigated. A comprehensive set of equations for the conservation of mass, momentum, and energy in the system was used for the calculation. An accurate assessment of thermodynamic and transport properties was performed to ensure accuracy and analyzed in detail.

The physical model is shown schematically in Figure 5. The test section is 70 cm long and has a diameter of 8.5 mm. The computational domain was simplified to an axisymmetric plane to focus on the study of heat transfer and other related phenomena.

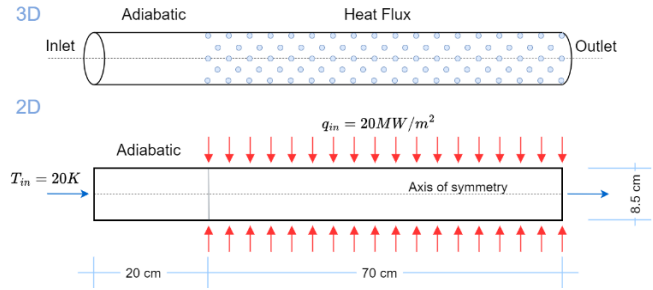

Figure 5. Schematic diagram of the model considered

A 20 cm long section at the beginning ensures that the flow field is stable before heat transfer takes place. A constant heat flux of 20 MW/m^2 was applied to the wall of the cooling channel. The mass flow rate at the inlet varies from 1,400 to 2,600 kg/m^{2}s. The coolant temperature at the inlet is 20 K; the coolant pressure at the outlet varies from 1.2 to 2.5 P_{cb}. All boundary conditions used in this simulation are described in Table 1.

Table 1. Boundary conditions

Parameter	Value
Coolant	Hydrogen
Mass flowrate [kg/s]	0.079 - 0.113 - 0.148
Inlet Temperature [K]	20
Outlet pressure [MPa]	1.56 - 1.95 - 2.60 - 3.25
Heat Flux [kW/m^2]	20

5.2 Sensitivity study

During the study, the cell count was documented at three different grid resolutions, which are shown in Figure 6. Table 2 shows the grid resolution in both the flow direction and the vertical direction. The resolution for each grid was determined according to the principle of consistent clustering. In the coarse grid, the y+ value (indicating proximity to the wall) was less than 2.0 for each cell near the wall, while it dropped to less than 1.0 in the medium and fine grids.

Figure 7 shows the changes in the maximum wall temperature and the pressure drop in the three grids. The data show that variations in grid resolution have only a minor influence on the wall temperature results. In particular, there is a clear difference in pressure drop between the coarse and medium grids, which then decreases between the medium and fine grids.

Table 2. Mesh analysis

LNG	Grid Size		y+
	Radial	Streamwise	
Coarse	15	2000	Coarse
Medium	30	4000	Medium
Fine	60	6000	Fine

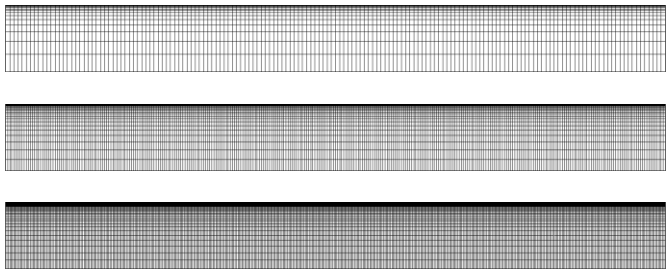

Figure 6. Mesh analysis

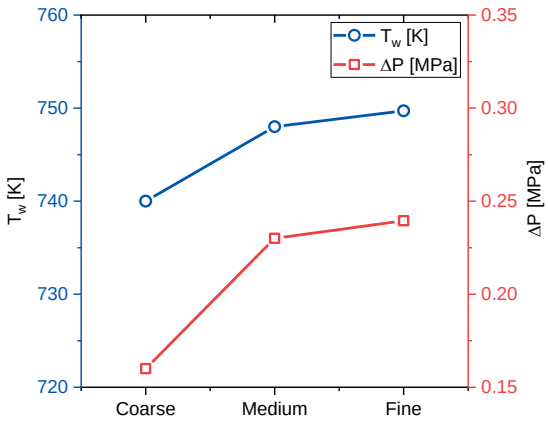

Figure 7. Sensitivity study

6. RESULT AND DISCUSSION

Under supercritical conditions, the behaviour of the fluid and its heat transfer properties can be significantly affected by the operating pressure. More specifically, variations in operating pressure have a remarkable impact on the thermophysical and transport properties affecting wall temperature and heat transfer, as shown in Figure 8. Higher operating pressures generally result in lower wall temperatures. In addition, a higher operating pressure can, for example, reduce the HTD. The maximum wall temperature was reduced by more than 11%, 21%, and 26% when the operating pressure was increased by 25%, 67% and 108%. Although the operating pressure was increased significantly, the HTD occurred. Under supercritical conditions, the Nusselt number can be significantly affected by changes in operating pressure. At higher pressures, the density and thermal conductivity of the fluid increase, as shown in Figure 1, while the specific heat capacity changes drastically near a critical point, as shown in Figure 2. These changes in fluid properties influence the convective heat transfer coefficient and affect the Nusselt number. In general, increasing the operating pressure increases the Nusselt number in the transcritical range and decreases the Nusselt number in the supercritical range, as shown in Figure 9.

The mass flow in a cooling channel plays an essential role in heat transfer. When supercritical hydrogen is used, it can

reduce the HTD and the wall temperature of the cooling channel. This study uses 1400, 2000, and 2600 kg/m^{2}s mass flow rates. The outlet pressure and inlet temperature are 1.2 P_{cr} and 20 K, respectively. Figure 10 shows that the flow becomes more turbulent with increasing mass flow rate, and the heat transfer coefficient initially increases due to the increasing mixing and turbulence.

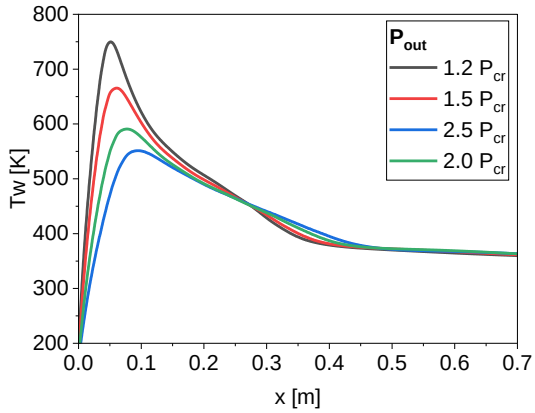

Figure 8. Distribution of wall temperature along the cooling channel for different operating pressures

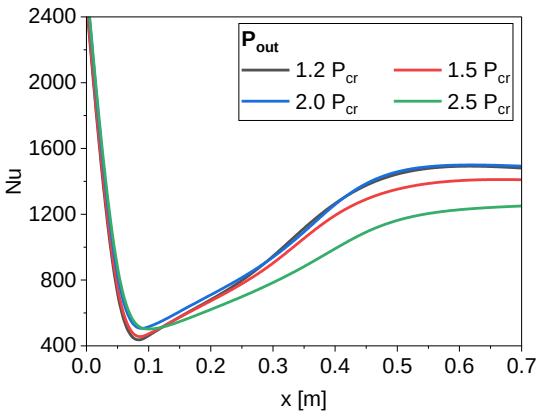

Figure 9. Variation of Nusselt number along the cooling channel for different operating pressures

However, a further increase in the mass flow can lead to an improvement in the heat transfer. The mass flow rate directly influences the wall temperature in a cooling channel. A higher mass flow leads to higher convective heat transfer rates, which can reduce the wall temperature. However, HTD can increase the wall temperature at meager mass flow rates. This is because the flow is less efficient at removing heat from the wall, resulting in higher temperatures. Figure 10 also shows that the wall temperature of the cooling channel is reduced by more than 26% and 36% when the mass flow rate increases by 43% and 86%, respectively.

The correlation between the Nusselt number and the mass flow rate in cooling channels at a specific pressure (P_{out} =1.2 P_{cr}) with transcritical hydrogen is shown in Figure 11. In transcritical cooling systems with hydrogen, the Nusselt number can be influenced by various parameters, including the mass flow rate. However, the specific relationship may depend on the design of the cooling channel, the operating conditions of the system, and the fluid properties. Increasing the mass flow rate can improve convective heat transfer, resulting in a higher Nusselt number near the critical hydrogen point. As a result, the wall temperature decreases, and the HTD becomes lower. It is important to note that transcritical cooling systems with hydrogen can be quite complex, and additional factors such as pressure, temperature, channel geometry, boundary conditions, and fluid properties also play a role in determining the Nusselt number. Therefore, a more detailed analysis would be required to establish an accurate relationship between the Nusselt number and the mass flow rate in a given transcritical hydrogen cooling system.

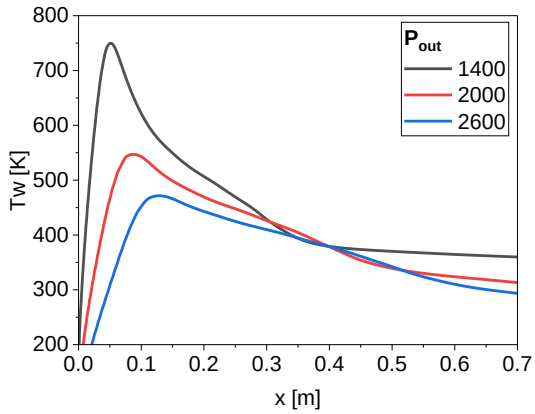

Figure 10. Distribution of wall temperature along the cooling channel for different operating pressures

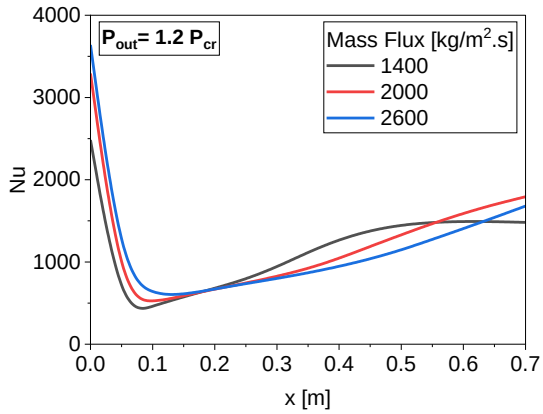

Figure 11. Variation of Nusselt number along the cooling channel at P_{out}=1.2 P_{cr} for mass fluxes considered

The effects of pressure drop and mass flow rate on the wall temperature and pressure drop in a circular pipe under transcritical conditions are shown in Figures 12 and 13. As the pressure drop increases, the fluid velocity in the pipe also increases. This higher velocity can increase frictional losses and turbulent flow, resulting in a more significant pressure drop along the pipe. In addition, a higher-pressure drop can reduce the hydrocarbon liquid's density, affecting the heat transfer properties and the wall temperature. Increasing the mass flow rate of the hydrocarbon fluid generally results in higher heat transfer rates as the fluid velocity increases, and there is more contact between the fluid and the pipe wall. As mentioned above, the increased mass flow rate can also lead to a higher pressure drop. However, the pressure drop can remain relatively constant if the pipe is designed for the increased flow.

Under transcritical conditions, changes in pressure and mass flow rate can significantly affect the wall temperature. An increase in pressure drop can lead to increased wall

temperature, primarily due to increased friction losses and changes in fluid properties. On the other hand, an increase in mass flow rate can help to dissipate heat more efficiently, resulting in lower wall temperatures. A deterioration in heat transfer can occur in transcritical flow regimes when the heat transfer coefficient decreases with increasing wall.

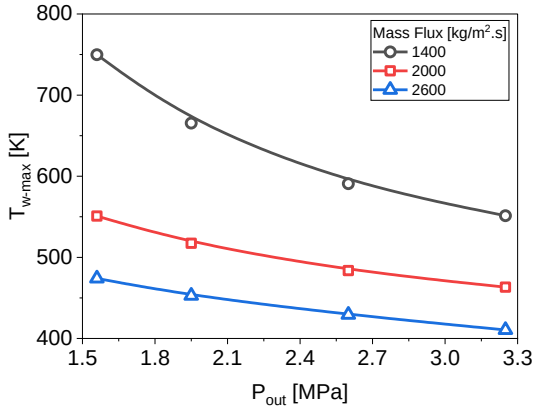

Figure 12. Variation of the maximum wall temperature of the cooling channel with operating pressures for mass fluxes considered

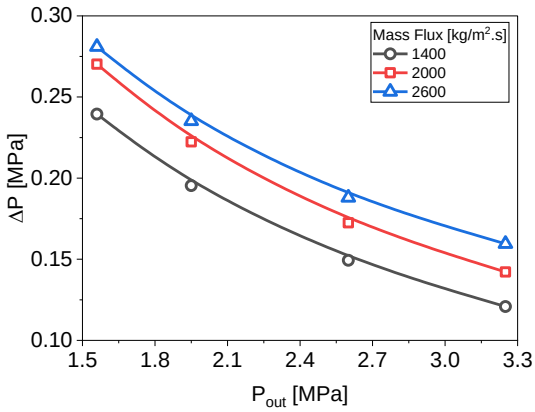

Figure 13. Variation of the pressure losses through the cooling channel with operating pressures for mass fluxes considered

Conditions with high-pressure drop and low mass flow rate can favor heat transfer deterioration, causing heat transfer efficiency to decrease and wall temperatures to increase. It is important to note that the exact effect of pressure drop and mass flow rate on wall temperature, pressure drop, and heat transfer deterioration varies based on factors like coolant properties, pipe geometry, and operating conditions.

It is worth noting that heat transfer deterioration can occur with transcritical hydrogen when the heat transfer coefficient decreases with increasing heat flux. This deterioration is influenced by factors such as the thermophysical properties of the hydrogen, the flow conditions, the tube geometry, and the surface properties.

The turbulent flow within the test section partitions into two distinct components. The first part represents the selected region within the small viscous sublayer, while the second represents the turbulent flow field. Based on these assumptions, the following formula calculates the heat transfer coefficient.

$$h_c = \frac{1}{R_v + R_t} \tag{19}$$

The thermal resistance in the core turbulent field is calculated as follows:

$$R_t = \frac{\delta_b \, Pr_t}{\mu_{t,b} \, c_{p,b}} \tag{20}$$

The operating pressure can considerably influence the thermal resistance in the turbulent core field, as shown in Figure 14. These curves exhibit similar patterns and rapid changes in the inlet and deterioration regions. The sharp transition in thermal resistance observed in the 1st part (x= 0-0.1 m) can be attributed to the persistent turbulence as the fuel absorbs heat. As the fuel temperature approaches a critical point, significant changes in physical properties lead to a critical region where thermal resistance undergoes a sudden shift and heat diffusion is limited. As a result, the abnormal elevate in wall temperature signifies the beginning of a deterioration in the behavior of the 2nd stage (x= 0.1-0.7 m). In essence, the phenomenon of HTD is closely linked to increased thermal resistance within the system.

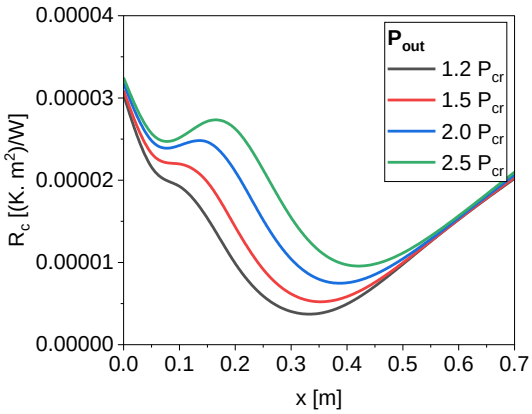

Figure 14. Variation of the thermal resistance in the core turbulent field along the cooling channel for different operating pressures

Higher operating pressures often lead to increased convective heat transfer within the core turbulence field. Higher pressures enhance fluid motion and turbulence, which improves heat transfer between the fluid and the solid surfaces. Consequently, the thermal resistance decreases. The operating pressure can influence the properties of the fluid, such as density and viscosity. Higher pressure generally leads to higher fluid density, which can affect heat transfer by changing flow patterns and velocity distribution. Higher viscosity at higher pressure can also affect convective heat transfer and lead to changes in thermal resistance. The operating pressure can affect the behavior of heat transfer surfaces such as heat exchangers or pipes. At higher pressure, the mechanical stresses on the surface can increase, leading to deformation or damage. This can affect the contact between the liquid and the solid surfaces, change the convective heat transfer, and ultimately influence thermal resistance.

7. CONCLUSIONS

The objective of this analysis is to study the heat transfer and flow resistance of hydrogen at supercritical pressures in a circular cooling channel. The simulation focused on a specific test case with a straight, circular cooling channel that has a

length of 0.7 m, a diameter of 0.415 cm, and a heat flux of 3 MW/m^2 directed into the radial wall of the cooling channel. The outlet pressure varied from 15.6 to 32.5 bar, and the inlet temperature was 25 K. The actual properties of the liquefied gas were calculated using the GERG-2008 equation of state and the ECS method. The numerical approach used three-dimensional finite volume solvers. The solver was validated using the experimental data of supercritical hydrogen. Under transcritical conditions, changes in pressure and mass flow rate significantly affected the wall temperature. At an operating pressure close to the critical point and low mass flow rates, there is a deterioration in heat transfer primarily due to local changes in the physical properties of the hydrogen near the heated surface. This phenomenon is characterized by a significant decrease in thermal conductivity and viscosity as the liquid approaches the wall. In contrast, the isobaric-specific capacity appears an evident peak near the tube walls, especially in the hydrogen layers. The specific heat demonstrates a clear peak at the pseudocritical point, indicating a critical transition in heat transfer behavior in these regions. Significant thermal resistance has a significant impact on the evolution of the deterioration behavior according to the area partitioning approach. The calculation of the convective heat transfer coefficient using the thermal resistance in the viscous sublayer and the turbulent core field plays a crucial role in HTD. In addition, a more detailed investigation of the flow and thermal properties of the viscous sublayer and the core field is required to better understand this phenomenon.

ACKNOWLEDGMENT

This research was financially supported by Al-Zaytoonah University of Jordan under Grant No. 40/17/2022-2023.

REFERENCES

[1] Nasser, I., Torres, Y., Santese, T., Haidn, O., Manfletti, C. (2023). A comprehensive investigation of heat transfer in a high aspect ratio cooling channel of a rocket engine using LNG coolant. Acta Astronautica, 213: 495-506. https://doi.org/10.1016/j.actaastro.2023.09.037

[2] Nasser, I., Haidn, O., Manfletti, C. (2023). Numerical investigation of rocket engine cooling channel heat transfer for different LNG under trans-critical conditions. International Journal of Thermofluids, 20: 100461. https://doi.org/10.1016/j.ijft.2023.100461

[3] Nasser, I., Manfletti, C., Santese, T., Haidn, O. (2023). A Comprehensive analysis of LNG as coolant in cooling channel of rocket engine under supercritical pressure conditions. In Aerospace Europe Conference 2023 – 10TH EUCASS – 9TH CEAS. https://doi.org/10.13009/EUCASS2023-404

[4] Elmouazen, H., Zhang, X.B., Gibreel, M., Ali, M. (2022). Heat transfer enhancement of hydrogen rocket engine chamber wall by using V-shape rib. International Journal of Hydrogen Energy, 47(16): 9775-9790. https://doi.org/10.1016/j.ijhydene.2022.01.045

[5] Elmouazen, H., Zhang, X.B., Gibreel, M., Ali, M. (2022). Numerical investigation of pentagonal V-shape ribs to enhance heat transfer in hydrogen rocket engine cooling channels. International Journal of Hydrogen Energy, 47(56): 23871-23886. https://doi.org/10.1016/j.ijhydene.2022.05.146

[6] Haemisch, J., Suslov, D., Oschwald, M. (2021). Experimental and numerical investigation of heat transfer processes in rocket engine cooling channels operated with cryogenic hydrogen and methane at supercritical conditions. Transactions of the Japan Society for Aeronautical and Space Sciences, Aerospace Technology Japan, 19(1): 96-105. https://doi.org/10.2322/tastj.19.96

[7] Tabazah, T., Hamdan, M.A., Deyab, O., Abdelhafez, E. (2014). Utilization of water produced hydrogen for domestic heating purposes. International Journal of Thermal & Environmental Engineering, 7(2): 95-99. https://doi.org/10.5383/ijtee.07.02.006

[8] Al-Oran, O., Shaban, N.A., Manna, R., Ayadi, O., A'saf, A., Lezsovits, F. (2024). Performance study of parabolic trough solar collector using hybrid nanofluids under Jordanian weather conditions. Journal of Thermal Analysis and Calorimetry, 149: 3981-3998. https://doi.org/10.1007/s10973-024-12961-8

[9] Li, X., Zhang, S.L., Bao, W., Qin, J., Haidn, O.J. (2022). Flow resistance characteristics of hydrocarbon fuel at supercritical pressure under various heat fluxes in regenerative cooling channel with micro-ribs. Aerospace Science and Technology, 131(A): 107999. https://doi.org/10.1016/j.ast.2022.107999

[10] Song, J., Liang, T., Li, Q.L., Cheng, P., Zhang, D.D., Cui, P., Sun, J. (2021). Study on the heat transfer characteristics of regenerative cooling for LOX/LCH4 variable thrust rocket engine. Case Studies in Thermal Engineering, 28: 101664. https://doi.org/10.1016/j.csite.2021.101664

[11] Shokri, M., Ebrahimi, A. (2018). Heat transfer aspects of regenerative-cooling in methane-based propulsion systems. Aerospace Science and Technology, 82-83: 412-424. https://doi.org/10.1016/j.ast.2018.09.025

[12] Ulas, A., Boysan, E. (2013). Numerical analysis of regenerative cooling in liquid propellant rocket engines. Aerospace Science and Technology, 24(1): 187-197. https://doi.org/10.1016/j.ast.2011.11.006

[13] Shaban, N., Nasser, I., Al Asfar, J., al-qawabah, S., Olimat, A. (2020). Thermodynamic and economic analysis of a refrigerator display cabinet equipped with a DC compressor and electronic expansion valve. International Journal of Heat and Technology, 38: 432-438. https://doi.org/10.18280/ijht.380219

[14] Pizzarelli, M., Battista, F. (2023). Oxygen–methane rocket thrust chambers: Review of heat transfer experimental studies. Acta Astronautica, 209: 48-66. https://doi.org/10.1016/j.actaastro.2023.04.028

[15] Xie, P.Y., Zhang, X.B. (2019). Hydrogen flow and heat transfer characteristic analysis in cooling channel wall with the spherical convexity structure. International Journal of Hydrogen Energy, 44(31): 16991-17003. https://doi.org/10.1016/j.ijhydene.2019.04.255

[16] Gibreel, M., Zhang, X.B., Elmouazen, H. (2023). Enhancement of heat transfer and hydrogen fuel flow characteristics in a wavy cooling channel with secondary branch design. International Journal of Thermal Sciences, 193: 108513. https://doi.org/10.1016/j.ijthermalsci.2023.108513

[17] Elmouazen, H., Zhang, X.B., Gibreel, M. (2023). Enhanced heat transfer and flow topology of hydrogen regenerative-cooling channels with novel X-shape ribs.

International Journal of Hydrogen Energy, 48(82): 32110-32124. https://doi.org/10.1016/j.ijhydene.2023.04.330
[18] Xie, P.Y., Zhang, X.B. (2020). Turbulent heat transfer analysis in supercritical hydrogen fuel flow considering thermal stratification. Numerical Heat Transfer, Part A: Applications, 77(10): 913-929. https://doi.org/10.1080/10407782.2020.1746566
[19] Sun, F., Li, Y., Sunden, B., Xie, G.N. (2019). The behavior of turbulent heat transfer deterioration in supercritical hydrocarbon fuel flow considering thermal resistance distribution. International Journal of Thermal Sciences, 141: 19-32. https://doi.org/10.1016/j.ijthermalsci.2019.03.027
[20] Haemisch, J., Suslov, D., Oschwald, M. (2019). Experimental study of methane heat transfer deterioration in a subscale combustion chamber. Journal of Propulsion and Power, 35(4). https://doi.org/10.2514/1.B37394
[21] Nasser, I., Martinez-Sanchis, D., Haidn, O., Manfletti, C. (2024). Impacts of hydrocarbons impurities on heat transfer deterioration. Applied Thermal Engineering, 246: 122894. https://doi.org/10.1016/j.applthermaleng.2024.122894
[22] Nasuti, F., Pizzarelli, M. (2021). Pseudo-boiling and heat transfer deterioration while heating supercritical liquid rocket engine propellants. The Journal of Supercritical Fluids, 168: 105066. https://doi.org/10.1016/j.supflu.2020.105066
[23] Pizzarelli, M. (2018). The status of the research on the heat transfer deterioration in supercritical fluids: A review. International Communications in Heat and Mass Transfer, 95: 132-138. https://doi.org/10.1016/j.icheatmasstransfer.2018.04.006
[24] Pizzarelli, M. (2016). A CFD-derived correlation for methane heat transfer deterioration. Numerical Heat Transfer, Part A: Applications, 69(3): 242-264. http://doi.org/10.1080/10407782.2015.1080575
[25] Pizzarelli, M., Urbano, A., Nasuti, F. (2010). Numerical Analysis of Deterioration in Heat Transfer to Near-Critical Rocket Propellants. Numerical Heat Transfer, Part A: Applications, 57(5): 297-314. https://doi.org/10.1080/10407780903583016
[26] Tong, J.F., Zhu, L.B., Lu, Y.P., Liang, T.J., Lu, Y.L., Wang, S.L., Yu, C.J., Dong, S.K., Tan, H.P. (2021). Study of flow and heat transfer for the supercritical hydrogen in spallation-type cylindrical neutron moderator. Energies, 14(18): 5856. https://doi.org/10.3390/en14185856
[27] Mardani, A., Barani, E. (2018). Numerical investigation of supercritical combustion of H_2-O_2. Energy & Fuels, 32(3): 3851-3868. https://doi.org/10.1021/acs.energyfuels.7b03025
[28] Zhang, L., Wang, E., Shi, J.F. (2024). Dynamic thermal performance of cryogenic liquid hydrogen heating from gas-liquid stratification to supercritical under a constant heat flux condition: A two-step simulation. International Journal of Hydrogen Energy. https://doi.org/10.1016/j.ijhydene.2024.02.025
[29] Hou, C.R., Ding, J.W., Yu, Y.S., Liu, X.D. (2024). Comparative molecular dynamics study of liquid hydrogen annular jets in subcritical and supercritical environments. International Journal of Hydrogen Energy, 51(D): 977-989. https://doi.org/10.1016/j.ijhydene.2023.07.111
[30] Manual, U. (2009). ANSYS FLUENT 12.0. Theory Guide, 67. https://www.afs.enea.it/project/neptunius/docs/fluent/html/th/main_pre.htm.
[31] Kunz, O., Wagner, W. (2012). The GERG-2008 wide-range equation of state for natural gases and other mixtures: An expansion of GERG-2004. Journal of Chemical & Engineering Data, 57(11): 3032-3091. https://doi.org/10.1021/je300655b
[32] Huber, M.L., Lemmon, E.W., Bell, I.H., McLinden, M.O. (2022). The NIST REFPROP database for highly accurate properties of industrially important fluids. Industrial & Engineering Chemistry Research, 61(42): 15449-15472. https://doi.org/10.1021/acs.iecr.2c01427
[33] Varzandeh, F., Stenby, E.H., Yan, W. (2017). Comparison of GERG-2008 and simpler EoS models in calculation of phase equilibrium and physical properties of natural gas related systems. Fluid Phase Equilibria, 434: 21-43. https://doi.org/10.1016/j.fluid.2016.11.016
[34] Rowland, D., Hughes, T.J., May, E.F. (2016). Extending the GERG-2008 equation of state: Improved departure function and interaction parameters for (methane+butane). The Journal of Chemical Thermodynamics, 97: 206-213. https://doi.org/10.1016/j.jct.2016.01.005
[35] Jiang, J.W., Prausnitz, J.M. (2000). Critical temperatures and pressures for hydrocarbon mixtures from an equation of state with renormalization-group theory corrections. Fluid Phase Equilibria, 169(2): 127-147. https://doi.org/10.1016/S0378-3812(00)00299-5
[36] Linstrom, P. (1997). NIST Chemistry WebBook, NIST Standard Reference Database 69. https://doi.org/10.18434/T4D303
[37] Gordon, S. (1994). Computer program for calculation of complex chemical equilibrium compositions and applications. NASA Reference Publication, 1(61): 1311. https://ntrs.nasa.gov/citations/19950013764
[38] Younglove, B.A., Ely, J.F. (1987). Thermophysical properties of fluids. II. methane, ethane, propane, isobutane, and normal butane. Journal of Physical and Chemical Reference Data, 16(4): 577-798. https://doi.org/10.1063/1.555785
[39] Younglove, B. (1982). Thermophysical Properties of Fluids: Argon, Ethylene, Parahydrogen, Nitrogen, Nitrogen Trifluoride, and Oxygen. American Institute of Physics. https://books.google.de/books?id=PZEfAQAAMAAJ.
[40] El-Tahry, S.H.E. (1983). K-epsilon equation for compressible reciprocating engine flows. J. Energy, 7(4). https://doi.org/10.2514/3.48086
[41] Friedman, R., Graham, R.W., Hendricks, R.C., Hsu, Y.Y. (1966). Experimental heat-transfer results for cryogenic hydrogen flowing in tubes at subcritical and supercritical pressures to 800 pounds per square inch absolute. https://ntrs.nasa.gov/citations/19660011645.

NOMENCLATURE

Cp	Isobaric heat capacity, J/(kg · °C)
k	Thermal conductivity, W/(m.K)
L	Length of test section, m

m	Mass flow rate, kg/s
Nu	Nusselt Number
p	Pressure, Pa
Pc	Critical pressure, Pa
q	Heat flux, W/m^2
T	Temperature, K
T_c	Critical temperature, K
x	x-axis, m
r	r-axis, m
y^+	Dimensionless wall distance

Greek characters

α	Dimensionless form of the specific Helmholtz energy
δ	Reduced mixture density
μ	Viscosity, Pa.s
μ_t	Turbulence viscosity, Pa.s
ρ	Density, kg/m^3
τ	Inverse reduced mixture temperature
τ_{ij}	Efficient deviatoric stress tensor

Subscripts

b	Bulk
cr	Critical point
i	x-coordinate
j	y-coordinate